# Rational Design of Inverted Nanopencil Arrays for Cost-Effective, Broadband, and Omnidirectional Light Harvesting

Hao Lin,[†,#] Fei Xiu,[†,⊥,#] Ming Fang,[†] SenPo Yip,[†,⊥] Ho-Yuen Cheung,[‡] Fengyun Wang,[§] Ning Han,[†,⊥] Kwok Sum Chan,[†,⊥,‖] Chun-Yuen Wong,[‡] and Johnny C. Ho[†,⊥,‖,*]

[†]Department of Physics and Materials Science and [‡]Department of Biology and Chemistry, City University of Hong Kong, 83 Tat Chee Avenue, Kowloon, Hong Kong, [§]The Cultivation Base for State Key Laboratory, Qingdao University, No. 308 Ningxia Road, Qingdao, People's Republic of China, [⊥]Shenzhen Research Institute, City University of Hong Kong, Shenzhen, People's Republic of China, and [‖]Centre of Functional Photonics (CFP), City University of Hong Kong, Tat Chee Avenue, Kowloon, Hong Kong. [#]These authors contributed equally to this work.

ABSTRACT
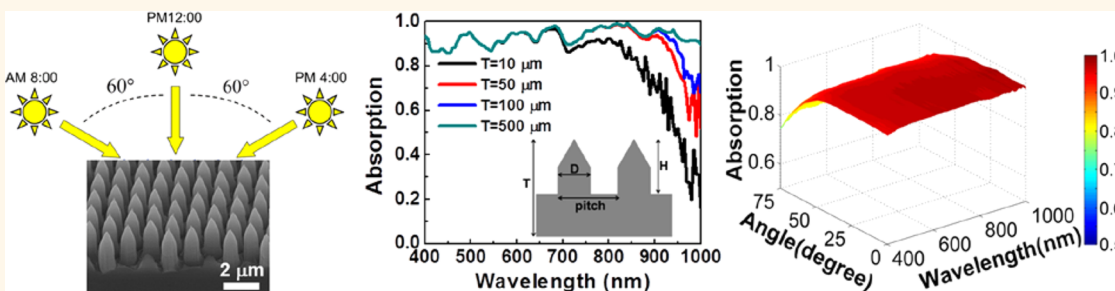
Due to the unique optical properties, three-dimensional arrays of silicon nanostructures have attracted increasing attention as the efficient photon harvesters for various technological applications. In this work, instead of dry etching, we have utilized our newly developed wet anisotropic etching to fabricate silicon nanostructured arrays with different well-controlled geometrical morphologies, ranging from nanopillars, nanorods, and inverted nanopencils to nanocones, followed by systematic investigations of their photon-capturing properties combining experiments and simulations. It is revealed that optical properties of these nanoarrays are predominantly dictated by their geometrical factors including the structural pitch, material filling ratio, and aspect ratio. Surprisingly, along with the proper geometrical design, the inverted nanopencil arrays can couple incident photons into optical modes in the pencil base efficiently in order to achieve excellent broadband and omnidirectional light-harvesting performances even with the substrate thickness down to 10 μm, which are comparable to the costly and technically difficult to achieve nanocone counterparts. Notably, the fabricated nanopencils with both 800 and 380 nm base diameters can suppress the optical reflection well below 5% over a broad wavelength of 400−1000 nm and a wide angle of incidence between 0 and 60°. All these findings not only offer additional insight into the light-trapping mechanism in these complex 3D nanophotonic structures but also provide efficient broadband and omnidirectional photon harvesters for next-generation cost-effective ultrathin nanostructured photovoltaics.

KEYWORDS: inverted nanopencils · nanocones · nanopillars · nanorods · broadband and omnidirectional light harvesting · wet anisotropic etching

I n recent years, due to the advent of nanotechnology, various three-dimensional (3D) silicon (Si) nanostructured arrays, such as nanowires, nanopillars, and nanocones, *etc*., have been extensively demonstrated for enhanced broadband and omnidirectional light harvesting.[1−8] All these 3D arrays can be considered as ideal light absorbers which can prolong the optical path length of incident light over the Lambertian limit by increasing the frequency of photons bouncing within the structure and minimizing the escape from the surface.[9] For the case of nanopillars, the increase of the light absorptive material filling ratio gives the increase of reflectance and the reduction of transmittance while the absorption depends strongly on the pillar diameter.[10] Dual- and later multidiameter nanopillars are then developed to

further improve the broadband absorption, with the smaller diameter tip to lessen the reflectance and the larger diameter base to maximize the effective absorption coefficient.[10,11] As the number of diameter segments increases, these nanopillars would resemble nanocones as optimal structures for the light absorption due to their graded transition of effective refractive index between the cones and air.[11] For example, in view of this unique advantage, Jeong *et al.* utilized these Si nanocones in combination with conductive polymer (PEDOT:PSS) to form hybrid solar cells with the resulting power conversion efficiency above 11%.[12] Importantly, the light-trapping effect which increases the optical path length becomes more profound for thinner Si.[12,13] Increasing this absorption in thin substrates is of the great importance to many technological applications, particularly for photovoltaics due to the enriched photon harvesting in all incident angles as well as the reduction of active material usage.[14] On the other hand, these 3D nanostructures can further increase the photogenerated carrier collection efficiency by separating the path for light absorption and carrier collection, as long as the radii of nanostructures or device thicknesses are smaller than the minority diffusion length.[15−17] Under such circumstances, the generation of photocarriers is substantial in the entire device thickness; this way, the 3D structure can facilitate the carrier separation and collection in the devices, and low-quality Si with poorer minority carrier diffusion lengths could be used because charge carriers can now diffuse over smaller distances for the collection.[18,19] These illustrate the significant dependence of the shape, dimension, and periodicity of these nanoarrays on their optical properties;[20,21] therefore, the rational design of Si nanostructures is certainly required for the practical implementation of high-performance and economically viable ultrathin Si photovoltaic devices.

Until now, much attention has been focused on Si nanocones and tapered nanostructures owing to the reduced reflection over a wide wavelength range through a graded effective refractive index.[19,22−24] However, a majority of these structures were fabricated with complicated and expensive reaction ion etching (RIE) processes, in which the extensive processing cost, fluorine contamination, and induced surface roughness/defects could demotivate the utilization of these nanoarrays for cost-effective applications.[25−27] Recently, we have demonstrated a low-cost wet-chemistry-only fabrication scheme for the controllable hierarchy of Si nanoarrays with different geometrical morphologies, ranging from nanopillars, nanorods, and inverted nanopencils to nanocones in large scale.[28] Here, we perform a more systematic investigation to further explore and understand the light coupling, propagation, and absorption nature of these nanoarrays, assisted with the optical simulations. It is found that optical properties of these

nanoarrays are predominantly governed by their geometrical factors comprising the structural pitch, material filling (base diameter-to-pitch) ratio and aspect (pillar height-to-base diameter) ratio, *etc*. Notably, along with the proper geometrical design, the inverted nanopencil arrays can couple incident photons into optical modes in the pencil base efficiently in order to achieve excellent broadband and omnidirectional light-harvesting performances, even with the substrate thickness down to 10 μm, which are comparable to the nanocone,[12] nanodome,[23] and nanopyramid[14] counterparts. Specifically, the fabricated nanopencils with both 800 and 380 nm base diameters can suppress the optical reflection well below 5% over a broad wavelength of 400−1000 nm and a wide angle of incidence between 0 and 60°. These findings not only offer additional insight into the light-trapping mechanism in these complex 3D nanophotonic structures but also provide efficient broadband and omnidirectional photon harvesters for the next-generation cost-effective ultrathin nanostructured photovoltaics.

RESULTS AND DISCUSSION

The 3D Si nanostructures were fabricated with an anisotropic wet etching technique as reported before.[28] Briefly, Si nanopillar arrays were utilized as fabrication templates prepared by a nanosphere lithography process followed by metal-assisted chemical etching (Supporting Information Figure S1). The templates were then treated with an [$AgNO_3$, HF, and HNO_3 or H_2O_2] etching system, and the etching mechanism originated from the site-selective deposition of Ag nanoclusters around the rim of the pillar tips. The tips were subsequently converted to truncated pillars by the treatment of HNO_3 to remove the Ag nanoclusters. Different etch anisotropies and aspect ratios (ARs) of these nanoarrays could be achieved by modulating the ratio and the components of the etching mixture. Figure 1 illustrates the schematics and scanning electron microscope (SEM) images of the as-fabricated nanopillars, nanorods, inverted nanopencils, and nanocones. The geometrical parameters of nanoarrays including the structural pitch, base diameter (*D*), and pillar height (*H*) are also depicted in the figure, while the symbol H1 designates the height of the pencil tip.

In order to quantitatively characterize optical properties of the nanostructures, the anti-reflection performance of these structures was evaluated with ultraviolet−visible (UV−vis) spectroscopy equipped with an integrating sphere in the wavelengths ranging from 400 to 1000 nm, as presented in Figure 2a. During the measurements, the angle of incidence (AOI) was fixed at 0° for the normal incident irradiation. As it can be clearly observed, arrays of these 3D nanostructures with the uniform height of ~2 um, diameter of ~800 nm, and pitch of ~1.27 μm demonstrate the superior anti-reflection properties as compared with
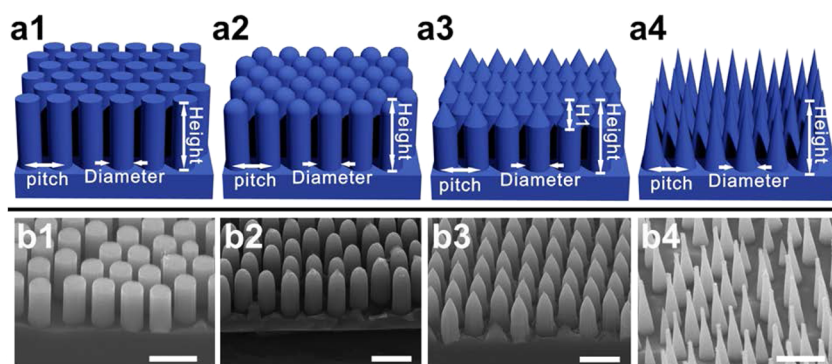
Figure 1. Schematic illustration of (a1) nanopillars, (a2) nanorods, (a3) inverted nanopencils, and (a4) nanocones studied in this work. The 45° tilted-angle-view SEM images of (b1) nanopillars, (b2) nanorods, (b3) inverted nanopencils, and (b4) nanocones. The structural pitches of all nanoarrays are 1.27 μm, and all scale bars are 2 μm.
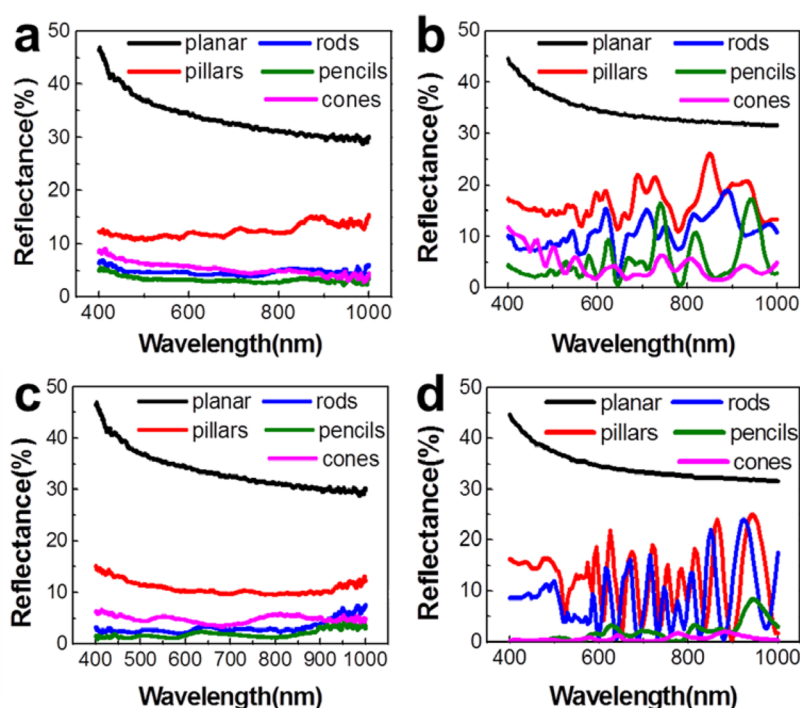

Figure 2. Comparison of the reflectance spectra of various nanostructured arrays between experimental measurement and optical simulation. (a) Experimental and (b) simulated spectra of different nanostructures with the pitch of 1.27 μm. (c) Experimental and (d) simulated spectra of different nanostructures with the pitch of 0.6 μm.

the planar Si substrate, which is not sensitive to the wavelengths of incoming light. Among all the structures, the inverted nanopencils exhibit the best anti-reflection behavior and the reflectance is depressed below 5% over the entire wavelength range. At the same time, optical simulations were performed to verify and understand the experimental results. Figure 2b gives the simulated optical reflection spectra of the same nanostructures. A similar trend is noticed where the inverted pencil and cone structures with the tapered shapes demonstrate lower reflection due to their graded refractive index profiles.[22,29−31] Notably, the experimentally measured reflectance of all four nanostructures is found to be slightly lower than those obtained from the simulations, which is mainly due to

the perfectly smooth surface considered in the simulations. The presence of surface roughness induced by the wet etching processes can further reduce the measured surface reflectance, suggesting the significant effect of surface roughness on the anti-reflection behavior here. Nanoarrays with the smaller pitch and pillar diameter of ∼0.6 μm and ∼380 nm, respectively, while maintaining the same pillar height of ∼2 μm and same material filling ratio (MFR) of ∼0.6, were also fabricated and assessed for the effect of different structural pitch on their optical properties (Figure 2c,d). It is obvious that the pencil and cone nanostructures illustrate the impressive anti-reflection properties with a little lower reflectance than the ones of large pitch structures because of the reduced spacing among
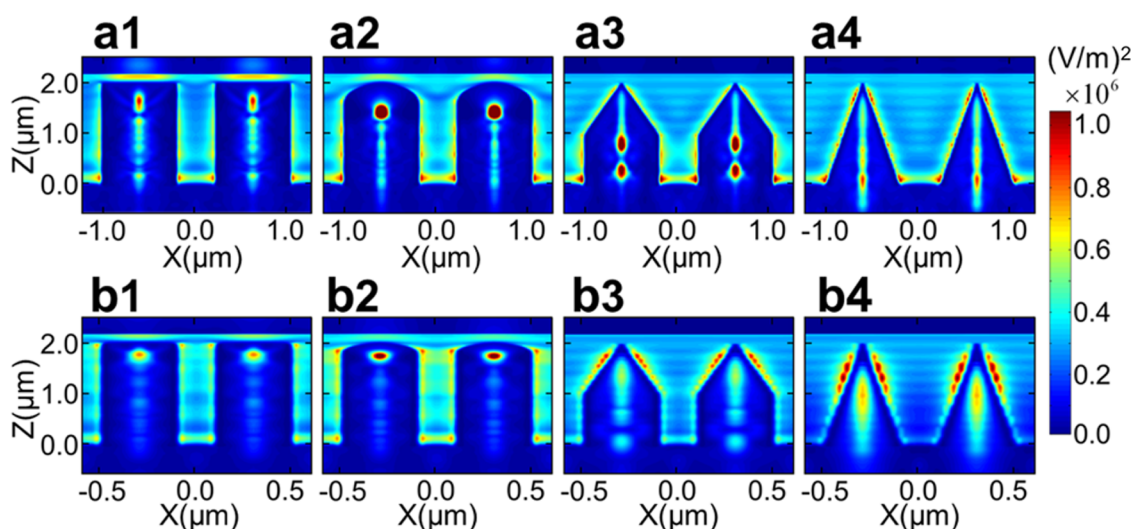
Figure 3. Two-dimensional solar-spectrum-weighted electrical field intensity contours of various nanostructures obtained by FDTD simulations. (a1−a4) Nanopillars, nanorods, inverted nanopencils, and nanocones with the pitch of 1.27 μm, base diameter (*D*) of 800 nm, and pillar height (*H*) of 2 μm, (b1−b4) nanopillars, nanorods, inverted nanopencils, and nanocones with the pitch of 0.6 μm, *D* of 380 nm, and *H* of 2 μm. The pencil tip height (H1) is 1 μm.

feature elements in the basal plane for the minimized bottom surface reflection. Simulation results also confirm the experimental data, while the oscillating features are believed to come from the interference of light throughout the 3D nanostructures with the periodicity matching.[3] These indicate the comparable photon-harvesting performance between inverted nanopencils and nanocones.

To further shed light to examine the propagation nature of light in various nanostructures, the solar-spectrum-weighted (300−1100 nm) electrical field intensity ($|E|^2$) distribution of the electromagnetic (EM) wave on the nanostructures was visualized and plotted in Figure 3. Figure 3a1−a4,b1−b4 demonstrates the simulated $|E|^2$ cross-sectional distribution through the center of nanopillars, nanorods, inverted nanopencils, and nanocones with the pitch of 1.27 and 0.6 μm, respectively. All these structures have the same height of 2 μm and MFR of ~0.6. In simulations, the EM plane waves propagate downward from $Z = 2.2\,\mu$m and reach the top surface of nanostructures at $Z = 2\,\mu$m. For the structures with 1.27 μm pitch, it is clear that there is relatively strong electrical field intensity on top of the nanopillars (Figure 3a1), indicating a significant reflectance due to the comparatively large surface area of pillar tips there. In contrast, a weaker field intensity is observed on top of the nanorods (Figure 3a2) with the same AR, while the pencil (H1 = 1 μm) and cone structures exhibit almost perfect anti-reflection on the top surfaces (Figure 3a3,a4). This suppressed reflectance could be interpreted as the effect of modulating the top surface morphologies from the planar to tapered shape and reducing the effective MFR in the tip region, which facilitates the minimal top surface reflection and efficient photon trapping plus transmission down to the base. Simultaneously, by comparing

the field distribution within the nanostructures, since the pencil tips can couple the field toward the pencil base, there exists substantial field intensity at the center of nanopencils, suggesting the higher probability of light absorption there as contrasted to the other three structures. However, relatively strong EM waves are also noticed propagating near the basal plane of these large pitch structures (Figure 3a1−a4), signifying the significant reflection from the bottom surfaces. In view of this, nanostructures with a smaller pitch of 0.6 μm and the MFR are also studied. As shown in Figure 3b1−b4, the field intensity decays quickly near the bottom surfaces of pillars and rods and nearly vanishes in the case of pencils and cones. This illustrates that the incident light has propagated effectively and the EM wave energy gets absorbed efficiently with the small pitch pencil and cone structures before the photons reach the bottom surface owing to the reduced basal open area. Notably, among all nanostructures investigated with the pitch of 0.6 μm, the nanocone structure gives the strongest field intensity at the center of cones, which is different from the case observed in nanostructures of 1.27 μm pitch. It is understood that, based on the same pillar height, base diameter, and MFR, nanopencils exhibit improved optical absorption over nanocones for the large pitch structures since the effective MFR is simply larger in the basal region of pencils for the enhanced photon trapping and absorption. Meanwhile, nanocones perform better for the small pitch structures because the effect of less open area for the minimized bottom reflection is more dominant such that the light can be absorbed by the cones more efficiently before hitting the basal plane.

In addition, the broadband-integrated (400−1000 nm) reflectance of various nanostructures (1.27 μm pitch)
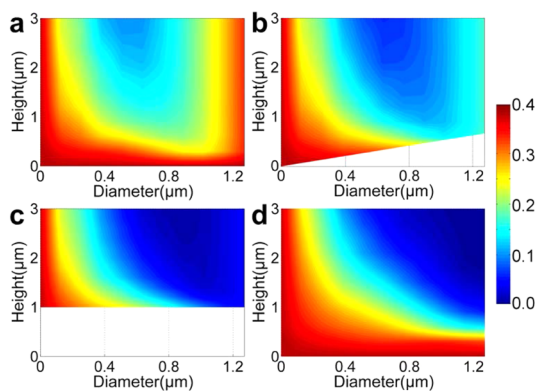
Figure 4. Two-dimensional simulated contours of broadband-integrated reflectance of various nanostructures as a function of the base diameter and pillar height: (a) nanopillars, (b) nanorods, (c) inverted nanopencils, and (d) nanocones. Pitch is 1.27 μm in all panels.

was also simulated as a function of base diameter (x-axis) and pillar height (y-axis) in order to investigate their geometrical effect on the light-trapping properties. As presented in Figure 4, the reflectance depends highly on the factors of AR and MFR based on a fixed pitch. It can be seen that significant reflection of photons occurs at small diameters for all the nanostructures studied, which is mainly due to the relatively large open basal area for the bottom reflection. For reducing this bottom reflection and achieving efficient light absorption, larger diameters or MFRs are desirable. However, when the pillar diameter is increased above 1 μm, the reflectance gets increased dramatically coming from the large reflective top surface area of pillar tips (Figure 4a). On the other hand, as compared with pillars, the nanorod structure with hemispherical tips displays the lower reflectance and extends the anti-reflection band (Figure 4b), which can be explained by the refractive index matching between the hemispheres and air in suppressing the light reflection.[32] It should be noted that the lower diagonal boundary in Figure 4b above the x-axis designates the hemispherical tip structure for each corresponding diameter. Apparently, nanorods demonstrate better optical anti-reflection than hemispherical structures with the same MFR since the basal spacing between the rods could effectively trap the photons for the improved light-harvesting capability. Moreover, the two-dimensional (2D) contours illustrate much better reflectance for both pencils and cones. Specifically, Figure 4d shows the reflectance of nanocones where, as the height increases and the diameter approaches the pitch, the reflectance would depress down to zero, becoming perfect anti-reflection of light. In other words, the lowest reflectance could be obtained when the Si substrate is fully covered by infinitely tall and continuous nanocone arrays, but it is technically challenging and economically ineffective to achieve this ideal structure. At the same time, the
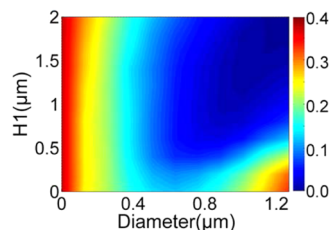
Figure 5. Two-dimensional simulated contours of broadband-integrated reflectance of inverted nanopencils as a function of the base diameter (D) and pencil tip height (H1). The pillar height (H) is 2 μm, and the pitch is 1.27 μm.

reflectance 2D contour of inverted nanopencils with H1 = 1 μm is depicted in Figure 4c, demonstrating that the anti-reflection band shifted to a slightly smaller diameter of 0.9 μm. The lower horizontal boundary indicates the nanocone structures with the height of 1 μm. In this pencil configuration, the excellent light-trapping behavior close to perfect anti-reflection can be obtained for the height larger than 2.2 μm and the diameter around 0.9 μm, which is contributed by the optimized minimal top surface reflection of tapered tips and maximal transmission of photons to basal pillars for the efficient absorption. Notably, this optimized geometry of nanopencil arrays can be easily and cost-effectively achieved through our anisotropic wet etching technique and experimentally confirmed in this work.[28] In any case, as the pencil diameter becomes larger toward the pitch, significant light reflection from the larger top surface would overwhelm the light trapping and the smaller spacing between the pencil elements would deter the transmission and propagation of photons down to the basal region. A similar trend is also observed for nanostructures with the smaller pitch of 0.6 μm (Supporting Information Figure S2). Furthermore, when the pitch is smaller than 0.3 μm, since the gap between nanoarrays becomes so small, there is no more coupling and propagation effect of light into the basal region; therefore, most of the light would just get bounced back for the increased reflection (Supporting Information Figure S3).

Instead of fixing the pencil tip (H1) at 1 μm, the broadband-integrated reflectance 2D contour of inverted nanopencils (1.27 μm pitch and 2 μm height) with different H1 and base diameter was also assessed. In terms of geometry, when H1 is 0, it is essentially the nanopillar structure; when H1 goes to the value of pillar height, it becomes the nanocone structure. In brief, as H1 increases from 0 to the pillar height, the nanopillar structure is first tapered, transforming into the inverted nanopencil configuration and then finally altered into nanocones. As given in Figure 5, for increasing H1, the corresponding nanopencil and nanocone structures demonstrate lower reflectance than the pillar counterparts, especially for the larger diameters or MFRs for the better light trapping, which is consistent with the results mentioned above. All of these have shown that
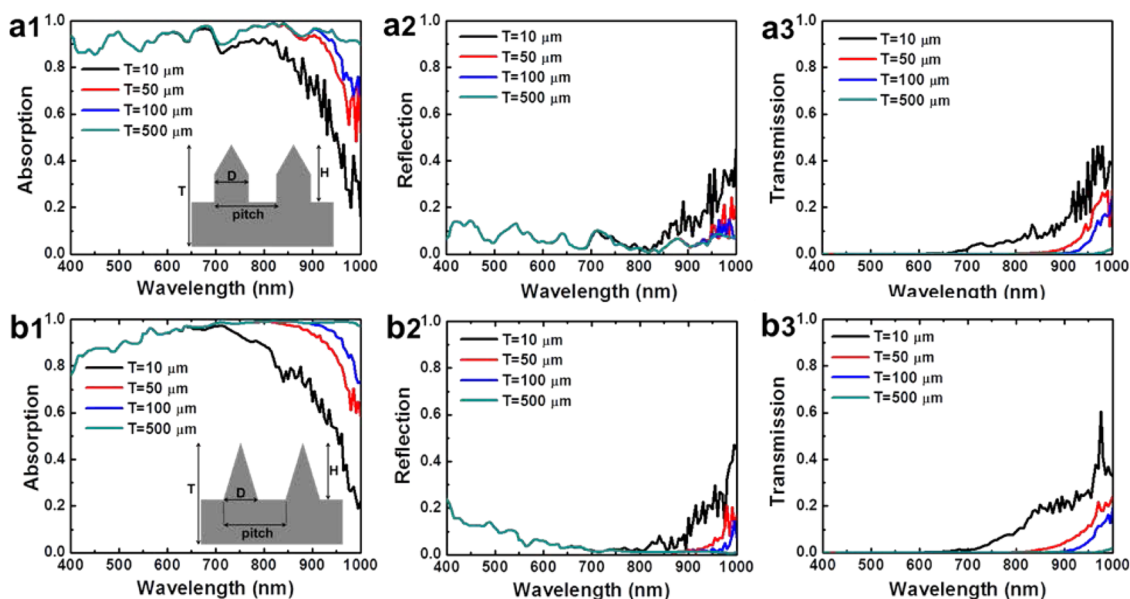
Figure 6. Simulation of optical properties for inverted nanopencils and nanocones with different substrate thickness. (a1) Absorption, (a2) reflection, and (a3) transmission data of nanopencils with the pitch of 1.27 μm, base diameter of 800 nm, pillar height of 2 μm, and pencil tip height of 1 μm. (b1) Absorption, (b2) reflection, and (b3) transmission data of nanocones with the pitch of 1.27 μm, base diameter of 800 nm, and pillar height of 2 μm.

properly designed nanopencils can exhibit excellent broadband light harvesting, comparable to the ideal nanocone structure. Similar to the cones but more manufacturable, the reflection suppression of these nanopencils is broadband as the index-matching is mostly wavelength-independent and higher aspect ratio is favorable to enable a smooth index transition from air to Si. More importantly, to achieve the effective anti-reflection, the periodicity of these nanoarrays needs to be in the subwavelength regime to utilize this effective averaged index.

In order to study these optical effects in more detail, simulations of optical properties for nanoarrays with different substrate thickness were performed in the diffraction mode. As shown in Figure 6a1,b1, the light absorption of nanopencils and nanocones are compared, respectively, with the pitch of 1.27 μm and four different thicknesses: 10, 50, 100, and 500 μm. It is evident that the 500 μm thick Si with the nanopencils and nanocones absorbed the visible light almost completely. These excellent light-trapping and anti-reflection properties are also confirmed even in thinner substrates, although there is a slightly higher reflection and transmission in the long wavelength region (Figure 6a2,a3,b2,b3). As the substrates become thinner, the light-trapping effect increasing the optical path length becomes more important, such that these tapered nanostructures can extend the light propagation for the more efficient absorption; however, since Si is intrinsically weak for absorption in the long wavelength range, it still requires decent substrate thickness for the effective absorption in the infrared or near-infrared region. When the substrates get thicker, the

light-trapping effect is less dominant as most of the light would get absorbed in a single pass such that the absorption is just merely dependent on the anti-reflection effect.[12] In any case, the light absorption improvements of these thin substrates with nanopencils are superior compared to that of thick planar Si substrates (Supporting Information Figure S4). Also, the consistent trend is similarly observed for the smaller pitch structures (Supporting Information Figure S5). All these results provide essential information for the design consideration of substrate thickness and indicate the inverted nanopencil structure being advantageous for solar cells with the ultrathin absorber layer.

For practical applications, such as photovoltaic devices, angular-dependent optical absorption is an important consideration for the maximization of corresponding energy conversion efficiency. Accordingly, the omnidirectional broadband characteristics of various nanostructures presented in Figure 1a1−a4 (pitch ~1.27 μm, height ~2 μm, and MRF ~ 0.6) with the incident irradiation angle ranging from 0 to 75° were studied and are depicted in Figure 7a1−a4. To have a direct observation of the absorption properties, absorption spectra were calculated by subtracting the experimentally measured values from unity as there is negligible transmission, especially for the visible light region for all substrate thicknesses, as discussed above. As shown in the 3D absorption contours, inverted nanopencils demonstrate the best absorption behavior among the structures over all incident angles and wavelengths, particularly for the small incident angles and long wavelength region. The broadband-integrated absorption of all structures was also
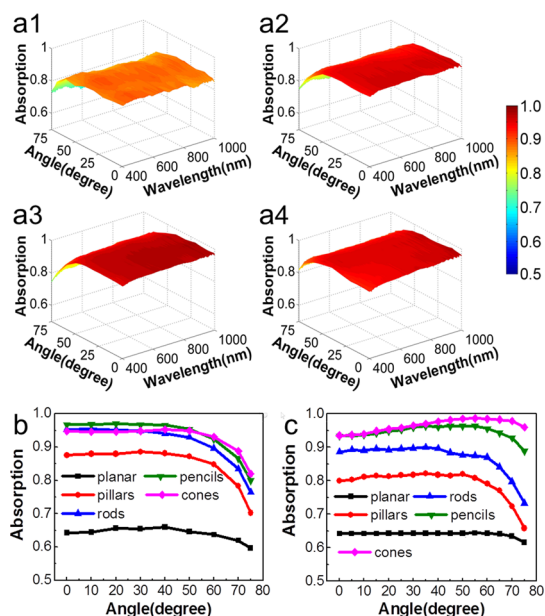
Figure 7. Comparison of the angular-dependent absorption of various nanostructured arrays between experimental measurement and optical simulation. (a1−a4) Three-dimensional contours of absorption spectra of nanopillars, nanorods, inverted nanopencils, and nanocones with the pitch of 1.27 μm and the pillar height of 2 μm. (b) Experimental and (c) simulated broadband-integrated absorption of different nanostructures as a function of the incident angle of irradiation.

measured and evaluated to understand the angular dependence more clearly. As presented in Figure 7b, all as-made structures including pillars, rods, pencils, and cones give the impressive omnidirectional photon-harvesting properties as compared with the planar Si. Specifically, the absorption of nanopencils and nanocones remains over 95% until an AOI of 60° is reached, in which these performances are comparable or better than the nanocone, nanodome, and nanopyramid arrays fabricated by complicated processing techniques. This deterioration in the absorption at large AOI is mainly attributed to the portion of photons entering the structures reduced significantly at such large angles, and thus the probability of light trapping is diminished, agreeing with the observation in Figure 7a3,a4. At the same time, simulations performed by diffraction mode were also carried out to verify the measurements, and the calculated light absorption of nanostructures is presented in Figure 7c. In general,

the simulated results are mostly consistent with the experimental trend, except the simulated absorption of pencils and cones is somewhat improved at large AOI between 30 and 60°. This is because, at the small incident angles, the photons are predominantly guided to enter the structures in an approximately vertical manner such that the optical reflection at the bottom surface is significant in these large pitch structures. At relatively larger angles, this bottom reflection is minimized owing to the enhanced light trapping that occurred in the tapered morphologies around the tips. For an AOI above 60°, eventually less photon can get into the features to result in less absorption, while these effects disappear for structures with the small pitch of 0.6 μm (Supporting Information Figure S6). Notably, this angular improvement is also not observed in the measurement (Figure 7b), which could again be due to the surface roughness without being considered in the calculations. Anyhow, all these have indicated that proper geometrically designed inverted nanopencil arrays can indeed achieve excellent broadband and omnidirectional light harvesting, which are analogous to the nanocone, nanodomes, and nanopyramid arrays.

CONCLUSION

In summary, we have not only illustrated a low-cost wet anisotropic etching technique for the fabrication of Si nanoarrays with different geometrical morphologies but also performed a systematic investigation further exploring and understanding light coupling, propagation, and absorption nature of these nanoarrays experimentally, assisted by optical simulations. It is revealed that optical properties of these nanoarrays are predominantly determined by their geometrical factors, such as the structural pitch, material filling ratio, and aspect ratio. Impressively, the properly designed inverted nanopencils can reduce the optical reflection below 5% over a broad wavelength range of 400−1000 nm and a wide angle of incidence between 0 and 60°, with the absorption performance comparable to the commonly accepted ideal but costly nanocone structures. This suggests the technological potency of these nanopencil arrays as efficient broadband and omnidirectional photon harvesters for next-generation cost-effective ultrathin nanostructured photovoltaics.

METHODS

Simulation Method. In simulations, the optical reflection of nanoarrays is calculated by the finite difference time domain (FDTD) method in R-Soft software. Plots of the refractive index values n and k of Si which we used in our simulations are shown in Supporting Information Figure S7. A uniform mesh of 20 nm × 20 nm × 10 nm was utilized, which is depicted in Supporting Information Figure S8. Perfectly matched layer boundary conditions were employed for the

upper and lower boundary of the simulation cell,[33] while periodic boundary conditions were used for the side boundaries to model the periodic nature of the arrays. In order to evaluate the anti-reflection properties of nanostructures as a function of height and diameter, their reflection spectra were integrated with the AM1.5G solar photon flux spectrum in the range of 400−1000 nm and plotted as two-dimensional contours. The above band gap broadband photon flux absorption with thickness and incident angle dependence of

nanostructures was calculated and plotted by the diffraction mode in R-Soft software.

Structural and Optical Characterization. Surface morphologies of fabricated nanoarrays were observed with SEM (FEI/Philips XL30). The optical properties were investigated by reflectance measurements (UV−vis−IR spectrometer, PE Lamda 750) performed at room temperature. Angular-dependent reflection measurements were performed with a custom-built 5 in. integration sphere apparatus, similar to the setup reported in ref 5. A xenon lamp was the light source to provide a broad wavelength range of 200−1100 nm, monitored by a spectrometer.

Conflict of Interest: The authors declare no competing financial interest.

Supporting Information Available: Process schematics of the formation of different nanoarrays; 2D simulated contours of broadband-integrated reflectance of various nanostructures with the pitch of 0.6 μm; simulated broadband-integrated reflectance of various nanoarrays with different pitch; simulation of optical properties for planar silicon with different substrate thickness as well as for inverted nanopencils and nanocones with the pitch of 0.6 μm and different substrate thicknesses; comparison of the broadband-integrated absorption of different nanostructures with the pitch of 0.6 μm between experiment and simulation; plots of the refractive index values *n* and *k* of Si utilized in the simulations; schematic illustration of the unit cell performed in the simulations. This material is available free of charge *via* the Internet at http://pubs.acs.org.

REFERENCES AND NOTES

1. Wang, H.-P.; Lin, T.-Y.; Hsu, C.-W.; Tsai, M.-L.; Huang, C.-H.; Wei, W.-R.; Huang, M.-Y.; Chien, Y.-J.; Yang, P.-C.; Liu, C.-W.; *et al.* Realizing High-Efficiency Omnidirectional n-Type Si Solar Cells *via* the Hierarchical Architecture Concept with Radial Junctions. *ACS Nano* **2013**, *7*, 9325–9335.

2. Lin, Q.; Hua, B.; Leung, S.; Duan, X.; Fan, Z. Efficient Light Absorption with Integrated Nanopillar/Nanowell Arrays for Photovoltaic Applications. *ACS Nano* **2013**, *7*, 2725–2732.

3. Leung, S.-F.; Yu, M.; Lin, Q.; Kwon, K.; Ching, K.-L.; Gu, L.; Yu, K.; Fan, Z. Efficient Photon Capturing with Ordered Three-Dimensional Nanowell Arrays. *Nano Lett.* **2012**, *12*, 3682–3689.

4. Wang, F.; Yang, Q. D.; Xu, G.; Lei, N. Y.; Tsang, Y. K.; Wong, N. B.; Ho, J. C. Highly Active and Enhanced Photocatalytic Silicon Nanowire Arrays. *Nanoscale* **2011**, *3*, 3269–3276.

5. Yu, R.; Ching, K.-L.; Lin, Q.; Leung, S.-F.; Arcrossito, D.; Fan, Z. Strong Light Absorption of Self-Organized 3-D Nanospike Arrays for Photovoltaic Applications. *ACS Nano* **2011**, *5*, 9291–9298.

6. Zhu, J.; Yu, Z.; Fan, S.; Cui, Y. Nanostructured Photon Management for High Performance Solar Cells. *Mater. Sci. Eng. Rep.* **2010**, *70*, 330–340.

7. Garnett, E.; Yang, P. Light Trapping in Silicon Nanowire Solar Cells. *Nano Lett.* **2010**, *10*, 1082–1087.

8. Dai, Y. A.; Chang, H. C.; Lai, K. Y.; Lin, C. A.; Chung, R. J.; Lin, G. R.; He, J. H. Subwavelength Si Nanowire Arrays for Self-Cleaning Antireflection Coatings. *J. Mater. Chem.* **2010**, *20*, 10924–10930.

9. Han, S. E.; Chen, G. Toward the Lambertian Limit of Light Trapping in Thin Nanostructured Silicon Solar Cells. *Nano Lett.* **2010**, *10*, 4692–4696.

10. Fan, Z.; Kapadia, R.; Leu, P. W.; Zhang, X.; Chueh, Y.-L.; Takei, K.; Yu, K.; Jamshidi, A.; Rathore, A. a; Ruebusch, D. J.; *et al.* Ordered Arrays of Dual-Diameter Nanopillars for Maximized Optical Absorption. *Nano Lett.* **2010**, *10*, 3823–3827.

11. Hua, B.; Wang, B.; Yu, M.; Leu, P. W.; Fan, Z. Rational Geometrical Design of Multi-diameter Nanopillars for Efficient Light Harvesting. *Nano Energy* **2013**, *2*, 951–957.

12. Jeong, S.; Garnett, E. C.; Wang, S.; Yu, Z.; Fan, S.; Brongersma, M. L.; McGehee, M. D.; Cui, Y. Hybrid Silicon Nanocone-Polymer Solar Cells. *Nano Lett.* **2012**, *12*, 2971–2976.

13. Wang, K. X.; Yu, Z.; Liu, V.; Cui, Y.; Fan, S. Absorption Enhancement in Ultrathin Crystalline Silicon Solar Cells with Antireflection and Light-Trapping Nanocone Gratings. *Nano Lett.* **2012**, *12*, 1616–1619.

14. Mavrokefalos, A.; Han, S. E.; Yerci, S.; Branham, M. S.; Chen, G. Efficient Light Trapping in Inverted Nanopyramid Thin Crystalline Silicon Membranes for Solar Cell Application. *Nano Lett.* **2012**, *12*, 2792–2796.

15. Yu, R.; Lin, Q.; Leung, S.-F.; Fan, Z. Nanomaterials and Nanostructures for Efficient Light Absorption and Photovoltaics. *Nano Energy* **2012**, *1*, 57–72.

16. Garnett, E. C.; Brongersma, M. L.; Cui, Y.; McGehee, M. D. Nanowire Solar Cells. *Annu. Rev. Mater. Res.* **2011**, *41*, 269–295.

17. Kelzenberg, M. D.; Boettcher, S. W.; Petykiewicz, J. A.; Turner-Evans, D. B.; Putnam, M. C.; Warren, E. L.; Spurgeon, J. M.; Briggs, R. M.; Lewis, N. S.; Atwater, H. A. Enhanced Absorption and Carrier Collection in Si Wire Arrays for Photovoltaic Applications. *Nat. Mater.* **2010**, *9*, 239–244.

18. Zhu, J.; Yu, Z.; Burkhard, G. F.; Hsu, C.-M.; Connor, S. T.; Xu, Y.; Wang, Q.; McGehee, M.; Fan, S.; Cui, Y. Optical Absorption Enhancement in Amorphous Silicon Nanowire and Nanocone Arrays. *Nano Lett.* **2009**, *9*, 279–282.

19. Wang, B.; Leu, P. W. Enhanced Absorption in Silicon Nanocone Arrays for Photovoltaics. *Nanotechnology* **2012**, *23*, 194003.

20. Chang, H. C.; Lai, K. Y.; Dai, Y. A.; Wang, H. H.; Lin, C. A.; He, J. H. Nanowire Arrays with Controlled Structure Profiles for Maximizing Optical Collection Efficiency. *Energy Environ. Sci.* **2011**, *4*, 2863–2869.

21. Wang, H. P.; Lai, K. Y.; Lin, Y. R.; Lin, C. A.; He, J. H. Periodic Si Nanopillar Arrays Fabricated by Colloidal Lithography and Catalytic Etching for Broadband and Omnidirectional Elimination of Fresnel Reflection. *Langmuir* **2010**, *26*, 12855–12858.

22. Lohmüller, T.; Helgert, M.; Sundermann, M.; Brunner, R.; Spatz, J. P. Biomimetic Interfaces for High-Performance Optics in the Deep-UV Light Range. *Nano Lett.* **2008**, *8*, 1429–1433.

23. Zhu, J.; Hsu, C.-M.; Yu, Z.; Fan, S.; Cui, Y. Nanodome Solar Cells with Efficient Light Management and Self-Cleaning. *Nano Lett.* **2010**, *10*, 1979–1984.

24. Klein, K. L.; Melechko, A. V.; Fowlkes, J. D.; Rack, P. D.; Hensley, D. K.; Meyer, H. M.; Allard, L. F.; McKnight, T. E.; Simpson, M. L. Formation of Ultrasharp Vertically Aligned Cu−Si Nanocones by a DC Plasma Process. *J. Phys. Chem. B* **2006**, *110*, 4766–4771.

25. Schmitt, S. W.; Schechtel, F.; Amkreutz, D.; Bashouti, M.; Srivastava, S. K.; Hoffmann, B.; Dieker, C.; Spiecker, E.; Rech, B.; Christiansen, S. H. Nanowire Arrays in Multicrystalline Silicon Thin Films on Glass: A Promising Material for Research and Applications in Nanotechnology. *Nano Lett.* **2012**, *12*, 4050–4054.

26. Morton, K. J.; Nieberg, G.; Bai, S.; Chou, S. Y. Wafer-Scale Patterning of Sub-40 nm Diameter and High Aspect Ratio (>50:1) Silicon Pillar Arrays by Nanoimprint and Etching. *Nanotechnology* **2008**, *19*, 345301.

27. Hsu, C.-M.; Connor, S. T.; Tang, M. X.; Cui, Y. Wafer-Scale Silicon Nanopillars and Nanocones by Langmuir−Blodgett Assembly and Etching. *Appl. Phys. Lett.* **2008**, *93*, 133109.

28. Lin, H.; Cheung, H.-Y.; Xiu, F.; Wang, F.; Yip, S.; Han, N.; Hung, T.; Zhou, J.; Ho, J. C.; Wong, C.-Y. Developing Controllable Anisotropic Wet Etching To Achieve Silicon Nanorods, Nanopencils and Nanocones for Efficient Photon Trapping. *J. Mater. Chem. A* **2013**, *1*, 9942.

29. Huang, Y.-F.; Chattopadhyay, S.; Jen, Y.-J.; Peng, C.-Y.; Liu, T.-A.; Hsu, Y.-K.; Pan, C.-L.; Lo, H.-C.; Hsu, C.-H.; Chang, Y.-H.; *et al.* Improved Broadband and Quasi-omnidirectional Anti-reflection Properties with Biomimetic Silicon Nanostructures. *Nat. Nanotechnol.* **2007**, *2*, 770–774.

30. Lee, Y.-J.; Ruby, D. S.; Peters, D. W.; McKenzie, B. B.; Hsu, J. W. P. ZnO Nanostructures as Efficient Antireflection Layers in Solar Cells. *Nano Lett.* **2008**, *8*, 1501–1505.

31. Zhu, J.; Yu, Z.; Burkhard, G. F.; Hsu, C.-M.; Connor, S. T.; Xu, Y.; Wang, Q.; McGehee, M.; Fan, S.; Cui, Y. Optical Absorption Enhancement in Amorphous Silicon Nanowire and Nanocone Arrays. *Nano Lett.* **2009**, *9*, 279–282.

32. Beckmann, P.; Spizzichino, A. *The Scattering of Electromagnetic Waves from Rough Surfaces*; Pergamon Press: Oxford, 1963.

33. Berenger, J.-P. A Perfectly Matched Layer for the Absorption of Electromagnetic Waves. *J. Comput. Phys.* **1994**, *114*, 185–200.